Mixed empirical-numerical method for investigating tunnelling effects on structures

Twana Kamal Haji[a,*], Alec M. Marshall[a], Andrea Franza[b]

[a]*Department of Civil Engineering, Faculty of Engineering, University of Nottingham, Nottingham, United Kingdom.*
[b]*Department of Engineering, University of Cambridge, Cambridge, United Kingdom.*

Abstract

The assessment of potential for building damage due to ground displacements caused by tunnelling is a global issue being faced by engineers. There is a two-way interaction between tunnelling and existing buildings; tunnel construction affects a building by inducing displacements in the soil underlying its foundation, and buildings influence tunnelling induced displacements via their weight and stiffness. Numerical analyses are widely used to investigate tunnelling and its impact on structures, however numerically predicted ground displacements are generally wider and shallower than those observed in practice. This paper presents a two-stage mixed empirical-numerical technique to estimate the effect of building stiffness on ground displacements due to tunnelling. In the first stage, greenfield soil displacements are applied to the soil model and the nodal reaction forces are recorded. In the second stage, the effect of tunnelling on a structure is evaluated by applying the recorded nodal reactions to an undeformed mesh. Results from conventional

*Corresponding author
Email address: twana.k.haji@gmail.com (Twana Kamal Haji)

numerical analyses of the problem are compared against those obtained using the mixed empirical-numerical approach. Results demonstrate the importance of imposing realistic inputs of greenfield displacements when evaluating structural response to tunnelling.
Keywords: Tunnelling, Displacement Prediction, Soil-Structure Interaction, Building Response

---

1. Introduction

As cities grow and urban infrastructure systems expand, the need for tunnels increases. Tunnel construction inevitably leads to the potential for ground displacements and damage to existing buildings and infrastructure. This paper focuses on the problem of how to evaluate tunnelling-induced movements within buildings. There have been many investigations of the effect of tunnelling on buildings. These studies include the influence of ground movements induced by tunnelling on both surface and subsurface structures. The interaction between a newly constructed tunnel and an existing building is a two-way relationship. The constructed tunnel affects the building by creating displacements in the soil underlying its foundation, and the existence of the building influences resulting soil movements. The effect of structural stiffness (Mair and Taylor, 1997; Franzius et al., 2006; Dimmock and Mair, 2008; Maleki et al., 2011; Farrell et al., 2014; Franza and DeJong, 2017) and building weight (Franzius et al., 2004; Giardina et al., 2015; Bilotta et al., 2017) have been shown to have an effect on the resulting ground movements.

Researchers have proposed several approaches to account for the effect of building stiffness in tunnel-structure interaction problems. Potts and Addenbrooke (1997) proposed a method based on the relative stiffness of a building compared to the underlying soil. They used 2D finite element (FE) analyses and considered several influential parameters of both the soil and the structure, such as material elastic moduli, building length, and cross sectional moment of inertia. This approach was extended by Franzius et al. (2006) who investigated the effect of structural stiffness on ground displacements in a 3D environment. The relative stiffness method was further examined by

researchers and new approaches have been proposed, some of which included the effect of building weight (Goh and Mair, 2014; Mair, 2013; Giardina et al., 2015).

In the analysis of Potts and Addenbrooke (1997) and Franzius et al. (2006), the effect of tunnelling on ground displacements was simulated within the FE model. The numerical simulation of a tunnel is an effective method for estimating tunnelling effects on buildings, however, FE methods generally predict a wider and shallower greenfield settlement trough than observed in practice (Mair et al., 1982; Augarde, 1997; Franzius et al., 2005, 2006; Jurecic et al., 2013). This issue can be overcome by the use of sophisticated soil constitutive models (Addenbrooke et al., 1997), however the input parameters for these models are generally not readily available. A wider/shallower input of greenfield displacements can affect the results of a soil-structure interaction analysis in two ways. First, for a given settlement trough shape, a smaller maximum settlement produces less distortions and therefore less damage to a building. Second, the width of the settlement trough can alter the response of the building; a building affected along its entire length will show less resistance to deformation compared to the same building subjected to ground displacements along part of its length. This feature, which relates to the effective end-fixity of the building, can be demonstrated using a beam analogy (Haji et al., 2018). A relatively long building extending further outside the ground displacement zone can be thought of like a beam with a relatively stiff support that constrains the rotation of the beam (similar to a fixed ended beam), whereas a shorter building behaves like a beam with a more flexible support that allows a degree of rotation (similar to a simply supported beam).

The aim of this paper is to describe the use of a two-stage mixed empirical-numerical (E-N) method to estimate the effect of the stiffness of a weightless building on ground displacements caused by tunnelling. In this method, realistic greenfield ground displacements, obtained from empirical or analytical relationships, are used as an input in a numerical analysis in order to determine the nodal reaction forces within the numerical mesh required to obtain the greenfield displacements (stage 1). The tunnel-building interaction is then solved in stage 2 by including the building within the model and applying the greenfield nodal reaction forces to the mesh. The applied numerical analysis adopts simple linear elastic constitutive soil behaviour; the effects of building weight on the tunnelling-induced response is therefore not considered in the analysis.

The paper begins with an overview of the relative stiffness approach, followed by a description of the adopted numerical analyses, including 'conventional' numerical analyses (in which the tunnelling process is simulated) and mixed E-N analyses. The purpose of the 'conventional' numerical analysis is to provide results for comparison which might be obtained by a practising engineer considering this problem, using reasonably standard numerical modelling methods. Results from the two numerical analyses are compared and the importance of having an accurate input of greenfield displacements in evaluating structural distortions is demonstrated.

2. Relative stiffness approach

Potts and Addenbrooke (1997) estimated the stiffness effect of a weightless structure on tunnelling induced ground movements in London clay. Based

on 2D numerical analyses, they represented the building as an elastic beam and proposed two relationships to estimate the relative bending and axial stiffness of the soil and the structure:

$$\rho^* = \frac{E_b I_b}{E_s \left(L_{bldg}/2\right)^4} \quad ; \quad \alpha^* = \frac{E_b A_b}{E_s (L_{bldg}/2)} \tag{1}$$

where ρ^* is the relative bending stiffness, α^* is the relative axial stiffness, E_b and E_s are the elastic moduli of the equivalent beam and the soil, respectively, I_b is the cross sectional moment of inertia of the equivalent beam, A_b is the cross-sectional area, and L_{bldg} is the length of the building perpendicular to the tunnel direction. For their plane strain problem, α^* is dimensionless but ρ^* has dimensions of m^{-1}.

Potts and Addenbrooke (1997) calculated the moment of inertia of the structure from that of each slab by employing the parallel axis theorem, with the centreline located in the middle of the building. An equivalent beam was then used to represent the building, which was designed such that it had a similar bending or axial stiffness as the building. Building damage parameters were proposed, referred to as the sagging and hogging deflection ratios (DR_{sag}, DR_{hog}), and compressive and tensile horizontal strains induced in the building (ε_{hc} and ε_{ht}), as shown in Figure 1. Subscripts $bldg$ and gf refer to $building$ and $greenfield$, respectively. The inflection point, i, of the settlement trough separates the zones of sagging and hogging. Strains were obtained directly from the output of the FE analyses at the neutral axis of the beam in order to eliminate bending effects. Potts and Addenbrooke

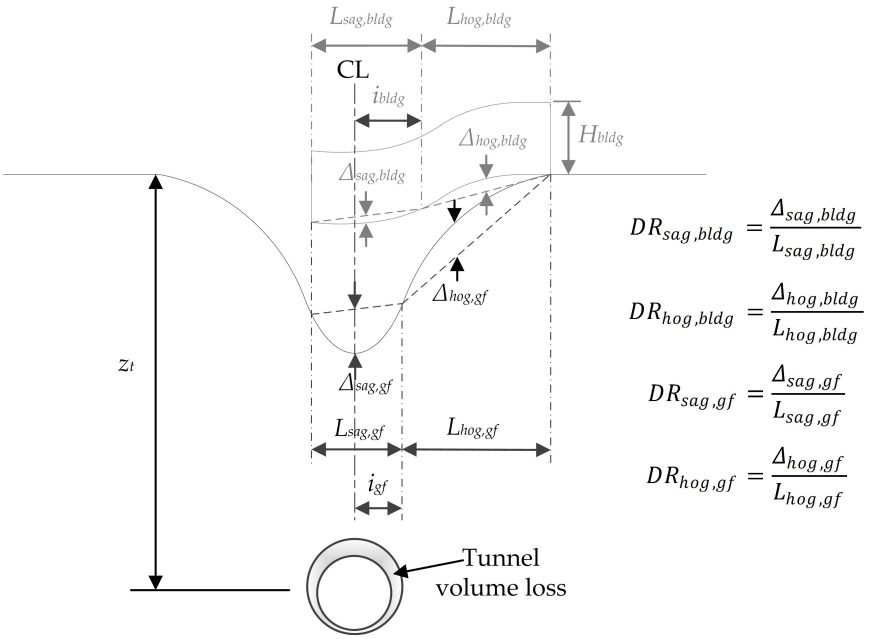

Figure 1: Transverse geometry of the interaction problem and deflection ratio parameters

(1997) suggested the following modification factors to relate the deflection ratios (Equation 2) and maximum horizontal strains (Equation 3) to the corresponding finite element greenfield situations:

$$M^{DR_{sag}} = \frac{DR_{sag,bldg}}{DR_{sag,gf}} \; ; \quad M^{DR_{hog}} = \frac{DR_{hog,bldg}}{DR_{hog,gf}} \tag{2}$$

$$M^{\varepsilon_{hc}} = \frac{\varepsilon_{hc,bldg}}{\varepsilon_{hc,gf}} \; ; \quad M^{\varepsilon_{ht}} = \frac{\varepsilon_{ht,bldg}}{\varepsilon_{ht,gf}} \tag{3}$$

where ε_h is maximum horizontal strain and the subscripts c and t denote compressive and tensile, respectively. The greenfield values relate to that portion of the greenfield settlement curve lying beneath the building.

Franzius et al. (2006) extended the relationships proposed by Potts and

Addenbrooke (1997) to 3D (i.e. including the effect of building width) and also considered the effect of tunnel depth in a more explicit fashion. They used the same principles for estimating building stiffness and represented the building by shell elements (rather than an actual 3D building). They suggested the following expressions for calculating bending and axial modification factors:

$$\rho^*_{mod} = \frac{E_b I_b}{E_s z_t L^2_{bldg} B_{bldg}} \quad ; \quad \alpha^*_{mod} = \frac{E_b A_b}{E_s L_{bldg} B_{bldg}} \tag{4}$$

where ρ^*_{mod} is the modified relative bending stiffness, α^*_{mod} is the modified relative axial stiffness, z_t is the tunnel depth and B_{bldg} is the building width parallel to the tunnel direction. It was shown that explicitly including tunnel depth in the relationship for ρ^*_{mod} provided a more realistic representation of bending response; this was not the case for the axial response described by α^*_{mod}.

Goh and Mair (2011) and Mair (2013) also proposed definitions of relative bending stiffness and design charts which were independent of tunnel-building eccentricity (whereas the previously adopted methods varied with eccentricity). Their methodology separates the building into sagging and hogging zones and estimates the relative bending stiffness independently for each part. This paper, however, adopts the methodology of Franzius et al. (2006) (Equation 4). Each method has its own advantages and limitations, however it was felt that treatment of the building as a single entity (as in the Franzius et al. (2006) method) was more logical for the analyses considered in this paper since the fixity condition of the building ends (which is misrepresented by splitting the building into parts) plays an important role.

3. Mixed empirical-numerical approach (mixed E–N)

To address the issues related to poor prediction of tunnelling induced settlement trough shape using numerical methods, yet still take advantage of the capabilities of numerical modelling for soil-structure interaction analysis, several authors have incorporated an empirical or analytical greenfield input into numerical analyses. Selby (1999) applied tunnelling induced ground surface movements to a finite element numerical model using Gaussian equations to estimate tunnelling effects on structures. Klar and Marshall (2008) applied Gaussian ground movements to all nodes of a finite difference numerical model in order to estimate tunnelling effects on pipelines. Wang et al. (2011) used a semi empirical method to investigate tunnelling effects on buried pipelines. The method of Selby (1999) and Klar and Marshall (2008) incorporated a two-stage analysis in which displacements are applied to the model in the first stage, and the reaction forces required to create the prescribed displacements are applied to the model in the second stage, after the structure is added to the model. In this way, the tunnelling process is not simulated directly in the numerical model, yet the soil-structure interactions caused by the greenfield input are simulated.

In the methodology presented in this paper, the two-stage analysis approach was adopted. The method is referred to as the mixed empirical-numerical (mixed E–N) method because an empirical/semi-analytical relationship was used for the greenfield input. In the first stage of the analysis, all nodes in the numerical mesh of the soil model are forced to displace according to the empirical functions (displacement input to the model) and the nodal reaction forces are recorded. Note that the numerical model in stage 1 inclu-

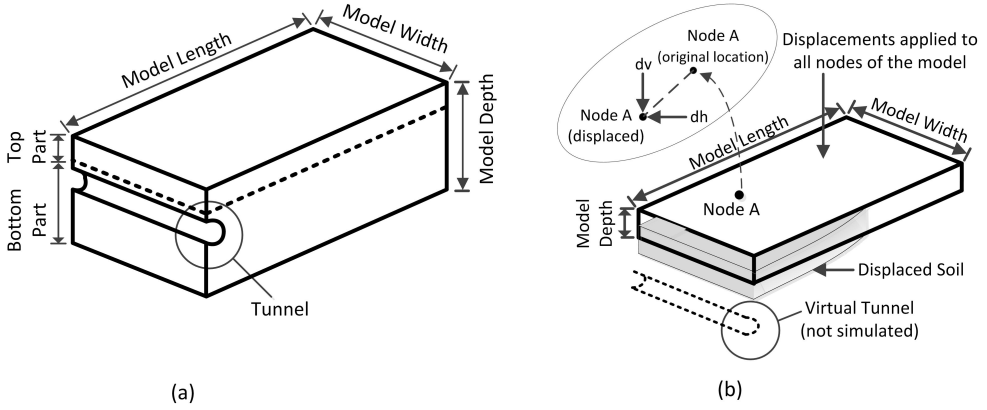

Figure 2: (a) Conventional numerical model and (b) mixed $E - N$ method

des elements that represent the soil and the building, however the elements associated with the building are not activated (i.e. a virtual building exists that does not affect the analysis). This ensures that no changes occur to the global model in stage 2 in terms of boundaries, dimensions and node numbering. In the second stage, the model is returned to its original condition and the structure is activated. The recorded nodal forces are then applied to all nodes of the soil model. Using this approach, the difference between the greenfield deformations and the deformations obtained when the structure is added represents the soil-structure interaction effect.

Results are provided from both conventional numerical analyses (Figure 2a), in which the greenfield displacements and soil-structure interactions were evaluated using the numerical model, as well as the mixed E–N method (Figure 2b). Only the soil depth above the tunnel, denoted by 'top part', is used for the mixed E–N analyses; the 'bottom part' is excluded.

The analyses presented here follow the procedure set out in Klar and Marshall (2008). The main difference is that the structure in this paper is a

3D beam of finite length (in the direction transverse to the tunnel direction) located on the surface, whereas for Klar and Marshall (2008) the structure was a buried pipeline of infinite length (achieved using appropriate boundary conditions). The assumptions inherent to the Klar and Marshall (2008) approach include: (1) the structure is continuous and always in contact with the soil, (2) both the soil and the structure are homogeneous linear elastic, (3) the tunnel is not affected by the existence of the structure, and (4) the soil responds to loading from the structure as an elastic half-space, disregarding the presence of the tunnel. In this paper, analyses were carried out considering both vertical and horizontal ground movements, thereby including both deflections and axial deformations of surface structures. A semi-analytical approach similar to that presented in Franza and Marshall (2015) was used to obtain the greenfield displacement input. Franza and Marshall (2015) modified the elastic analytical solution of Verruijt and Booker (1996) for an incompressible soil by introducing a corrective term, ζ. They obtained a closed-form solution that was able to represent greenfield displacements around a tunnel in sand based on data obtained from geotechnical centrifuge testing. The semi-analytical solution for horizontal (S_h) and vertical (S_v) greenfield displacements used in this paper are presented in Appendix A. Note that any input of greenfield displacements can be incorporated into this analysis methodology.

In Klar and Marshall (2008), the base of the mesh was forced to displace according to the input greenfield displacements even when the equivalent nodal forces were applied in the second stage of the analysis. This approach requires that the base of the mesh is not affected by the existence of the

included structure (i.e. by the loading due to soil-structure interaction), which was the case for the Klar and Marshall (2008) analysis. This approach creates issues for analyses of structures above relatively shallow tunnels. This paper proposes a method to address this constraint by using the following technique. As shown in Figure 2a, the targeted part of the soil is located above the tunnel crown. Instead of applying fixities and imposing greenfield displacements to the base of the model in stage 2 of the analysis, a 'base layer' is added to the bottom of the model (illustrated in Figure 3) which has the same properties as the top (target) layer (or could include other properties in the case of layered soil analyses) and is fixed in the vertical direction along its bottom. In this way, the soil responds to soil-structure interaction loading (i.e. reaction forces applied by the structure to the soil due to structure stiffness and distortions) in a way similar to an elastic half-space.

In stage 1, soil nodes within the whole target layer of the mesh are moved according to the greenfield displacements, while movements in the base layer are not imposed; they depend on the displacements applied to the target layer and the properties of the soil. The equivalent nodal forces from the target layer are then recorded and, in stage 2, after resetting the mesh displacements and adding the structure, the nodal forces in the target layer are applied to the mesh. It will be shown later that the use of the base layer provides an effective method for evaluating the effect of a structure on the entire depth of the target layer (Figure 3).

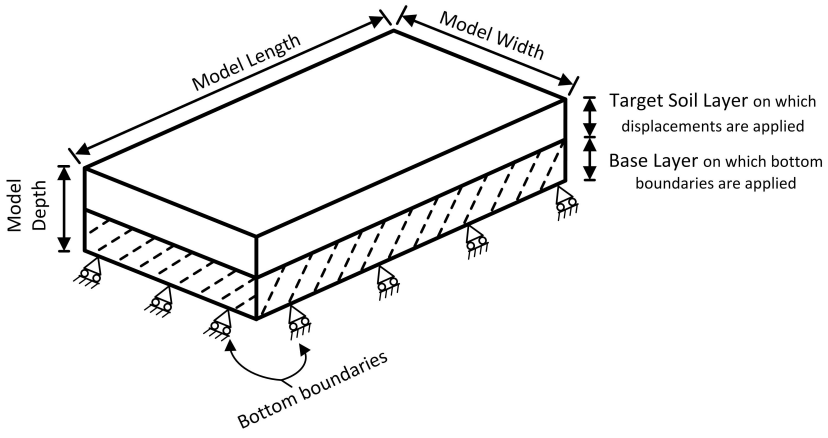

Figure 3: Mixed E–N model with base layer

4. Finite element software and material properties

The ABAQUS finite element software (SIMULIA, 2012) was used for both the conventional and mixed E–N analyses. All soil and building parts were created using 3D 8-node linear brick, solid elements (C3D8R) with reduced integration to relieve shear lock. The system was considered as a 2D problem; the effect of tunnel advancement was not included and the building was considered as a beam.

For the conventional numerical analysis, the soil was modelled as an elasto-plastic material with a Mohr-Coulomb failure criterion, having a Young's modulus of E_s=35 MPa, a Poisson's ratio of 0.25, a friction angle of 35°, a dilation angle of 1/4 of the frictional angle, a cohesion of 5 kPa to avoid analysis divergence, a density of 1600 kg/m^3, and a lateral earth pressure coefficient (K_0) of 0.5. In the elastic mixed E–N method, the same elastic soil parameters were used. For simplicity, E_s was kept constant for all modelled scenarios. Soil parameters were chosen to reasonably match the properties of

the fine sand (Fraction E Leighton Buzzard silica sand) used in the centrifuge tests of Marshall et al. (2012), Zhou (2014), and Franza (2016) (on which the semi-analytical greenfield displacement inputs used in this paper were based). Values of Poisson's ratio for medium to dense sands range from 0.2 - 0.4. A value of 0.25 was adopted in the numerical analyses presented here; this value has been assumed in various numerical analyses of experiments using Fraction E sand (Marshall et al., 2010; Giardina et al., 2015). Based on triaxial test data, Zhao (2008) found that the Young's modulus of Fraction E sand ranged from about 25 MPa to 105 MPa (at 1×10^{-2} axial strain for confining stresses between 100 and 400 kPa). In the analyses presented here, a value of 35 MPa was assumed as a representative value for the elastic modulus throughout the soil depth.

For the plastic parameters, the angle of friction of sands generally ranges from 30° to 40° for loose to dense sands (Bowles, 1997). A value of 35° was used in this work, which is close to the critical state value of 32° measured for Fraction E sand (Tan, 1990). The dilation angle of very dense sand can reach up to about 15° (Vermeer and Borst, 1984); for the analyses presented here a dilation angle of 9° was used. A coefficient of lateral earth pressure of $K_0 = 0.5$ was used, which is a typical assumption in the analysis of centrifuge experiments with normally consolidated sand (Marshall et al., 2010).

The building was modelled as an equivalent beam with a modulus of elasticity of 23 GPa, a Poisson's ratio of 0.15, and a varying height.

5. Model description

5.1. Conventional numerical model

In the conventional numerical analyses, a 4.65 m diameter tunnel was modelled within a soil domain $43D_t$ long and $10D_t$ deep, as illustrated in Figure 4. A unit length mesh was used in the direction of the tunnel axis. Two tunnel depths were considered, with C/D_t=2.4 and 4.4, as well as three relative tunnel-building eccentricities, $e/L_{bldg} = 0.0,\ 0.5$ and 0.75. A 60 m long building (also 1 m wide in direction of tunnel axis) was attached to the soil surface using a tie constraint (does not allow slip or separation). Equation 4 was used to evaluate ρ^*_{mod} and α^*_{mod}. Five buildings were analysed, as described in Table 1. The flexural and axial rigidity of the buildings, EI and EA, were chosen based on realistic values presented by Farrell (2011). The properties were selected so that they include low, medium and high stiffness structures.

Table 1: Building properties for conventional numerical and mixed E–N simulations

Cases	Beam thickness, t_B (m)	EI (kNm^2/m)	EA (kN/m)
1	0.10	1.9×10^3	2.3×10^6
2	0.25	3.0×10^4	5.8×10^6
3	0.50	2.4×10^5	1.2×10^7
4	1.00	1.9×10^6	2.3×10^7
5	3.00	5.2×10^7	6.9×10^7

The displacement controlled method described by Cheng et al. (2007), where increments of contraction are induced along the tunnel periphery, was used to simulate the tunnelling process. An oval-shaped pattern was assumed for the displacements around the tunnel, where maximum settlements occur at the tunnel crown and no movements occur at the invert, as shown in

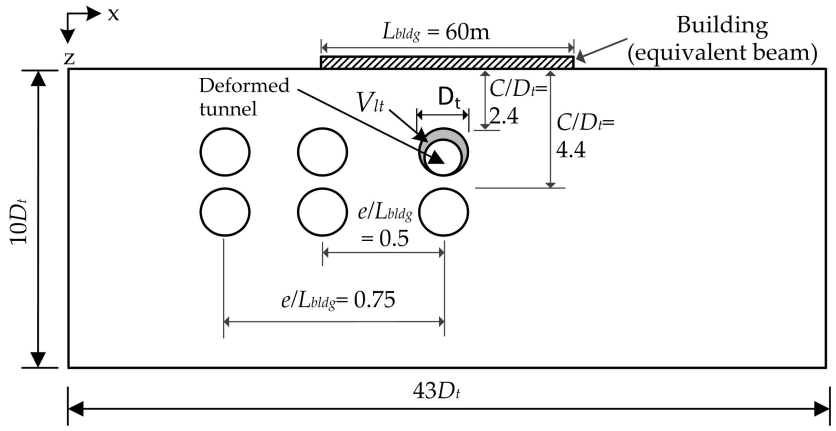

Figure 4: Illustration of numerical model showing dimensions, depths and locations of the tunnel

Figure 4. Tunnel boundary displacements were directed towards the centre of the converged tunnel. In the work of Marshall and Franza (2017) and Zhou (2014), experimental evidence was provided to show that, for tunnelling in dry sands, the tunnel volume loss concentrates at the top half of the tunnel while soil movements at the tunnel springline are small. The oval-shaped tunnel contraction boundary condition was therefore judged to be representative of the actual tunnel volume loss distribution that occurred during the centrifuge experiments.

Three cases of tunnel volume loss were considered for each tunnel/building scenario, as listed in Table 2. The chosen values of tunnel volume loss (V_{lt}) are based on the available centrifuge test data. In the numerical model, displacements of the tunnel boundary were increased until the volume loss at the surface in the greenfield situation matched that of $V_{ls,surf}$ in Table 2. This was done to ensure a fair comparison of numerical results with those from the mixed E–N since the most important zone is at the surface where

the tunnel-building interaction takes place.

5.2. Mixed E–N model

In the mixed E–N analyses, a soil model of the same dimensions as the conventional numerical model was used. The analyses, summarised in Table 2, were based on centrifuge experiment data. The input of the tunnelling induced greenfield displacements to the mixed E–N model was obtained using Equations 5, 6, and 8 in Appendix A. The depth of the target and base layers for both tunnel depth cases (C/D_t = 2.4 and 4.4) were 10 m and 35 m, respectively, except for simulations where the effect of the size of the base layer was investigated. Three tunnel volume losses (V_{lt}) of 0.96%, 1.76% and 3.94% were considered; these result in the soil volume losses ($V_{ls,surf}$) at the ground surface shown in Table 2. The considered soil relative density was I_d= 90% for all simulations. The element types and elastic properties of the soil and the building were the same as the conventional numerical model.

Table 2: Summary of numerical analyses: tunnel (V_{lt}) and surface soil volume losses ($V_{ls,surf}$)

C/D_t	I_d (%)	V_{lt} (%)	$V_{ls,surf}$ (%)
2.4	90%	0.96	0.92%
2.4	90%	1.76	1.55%
2.4	90%	3.94	2.50%
4.4	90%	0.96	1.68%
4.4	90%	1.76	2.77%
4.4	90%	3.94	4.40%

6. Mixed E–N model results

6.1. Greenfield input

In addition to predicting a wide settlement trough, conventional numerical methods are also not able to replicate the complex distribution of soil volume loss that occurs above a tunnel in a drained granular soil, where shear strains can lead to contraction or dilation of the soil. The amount of contraction/dilation of the soil, which depends on its relative density, the depth of the tunnel, and the magnitude of tunnel volume loss, ultimately leads to a change in the shape of the settlement trough (Marshall et al., 2012; Zhou et al., 2014). This necessitates the use of more complex empirical relationships compared to the standard Gaussian curve generally applied to settlements above tunnels in clay.

Figure 5 shows greenfield vertical and horizontal displacements for the conventional numerical and mixed E–N models for $C/D_t = 2.4$. The centrifuge test data, on which the semi-analytical expressions (and therefore mixed E–N analyses) are based are also illustrated. The figure presents data at two depths ($z/z_t = 0.0$ and $z/z_t = 0.37$) and at two values of surface volume loss ($V_{ls,surf}$=1.55% and 2.5%). The vertical displacement data illustrate the wide/shallow settlement trough obtained using the conventional numerical model. For horizontal displacements at the surface, the magnitude of maximum horizontal displacement from the conventional numerical analyses is considerably less than the experimental data, and occurs much further away from the tunnel. It will be demonstrated later that the width of the greenfield displacements has an important impact on the outcomes of soil-building interaction analyses. The building in the conventional numerical model will

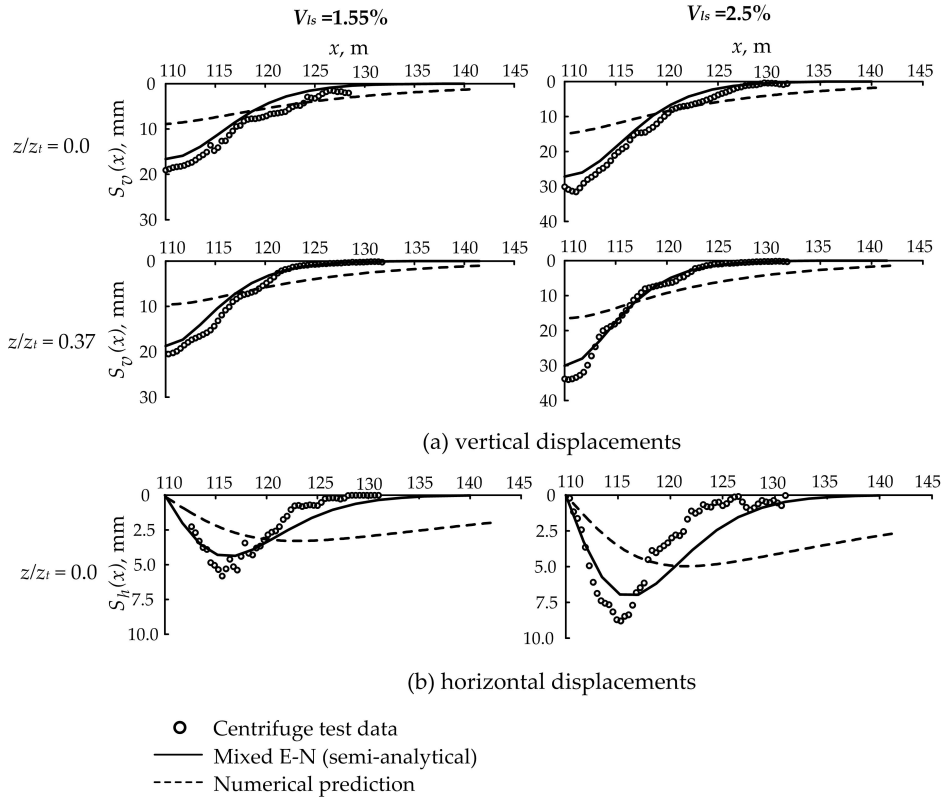

Figure 5: Tunnelling induced greenfield ground displacements for $C/D_t = 2.4$: (a) vertical, (b) horizontal

be subjected to ground displacements along a greater length compared to reality (assuming that the centrifuge test data gives a good representation of 'reality'). The semi-analytical expressions are shown to give a good fit to the centrifuge data, hence there is good confidence that the greenfield inputs into the mixed E-N interaction analyses reflect what is expected in reality.

6.2. Effect of base layer thickness

Figure 6 shows the effect of base layer thickness on the mixed E-N results for different building cases (Table 1) at a tunnel volume loss of 1.76% and

tunnel depths corresponding to $C/D_t = 2.4$ and 4.4. The thickness of the base layer was varied from 5 to 35 m. Results based on the approach of Klar and Marshall (2008) in which the base of the model (target layer thickness = 10 m with no base layer) was assumed to follow greenfield displacements are also included. Figure 6a illustrates that displacements decrease with the increase of the base layer thickness. The maximum displacements are greatest when there is no base layer (i.e. the Klar and Marshall (2008) case). The effect of the base layer was constant for values of thickness greater than 25 m (data coincides with base layer = 25 m line). The larger displacements for the less thick base layer cases is caused by the effect of the constraint at the bottom of the base layer, which prevents the reduction of downwards movements near this boundary. Since the first stage of the analysis is a displacement controlled process in which all soil nodes in the top part are forced to displace by a certain amount, relatively large reaction forces are created in the nodes, including the effect of the applied displacements as well as the bottom boundary. When the structure is added to the analysis in stage 2, these nodal reactions force the building to displace more compared to the larger base layer thickness cases due to the extra reaction forces created by the effect of the nearby bottom boundary.

The stiffness of the building also has an impact on the soil-building interaction. Figure 6b shows that the base layer thickness has little effect when it is greater than 5 m for the more flexible equivalent beam in building case 2, where the beam thickness t_B is 0.25 m. In the case of a fully flexible building, the base layer effects are negligible. The stiffer the building, the greater the required thickness of the base layer.

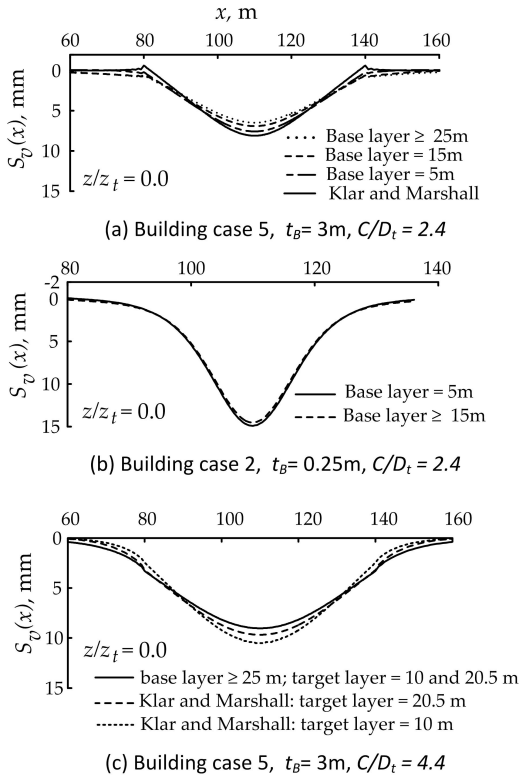

Figure 6: Effect of base layer thickness on soil-building interaction: $V_{lt} = 1.76\%$

For deeper tunnels, the effect of the bottom boundary on the soil-building interaction reduces since the influence of the building at the base of the target layer is not as significant. Figure 6c shows three simulations in which the thickness of target layer was either 10 or 20.5 m for a tunnel depth corresponding to $C/D_t = 4.4$ and building case 5 ($t_B = 3$ m). The mixed E–N analysis with a base layer of 25 m provided the same result for both target layer thicknesses. The Klar and Marshall (2008) results are shown to match more closely with the mixed E–N results as the thickness of the top layer is increased.

6.3. Interaction effects of horizontal and vertical displacements

The analyses presented here consider the effect of both vertical and horizontal greenfield displacements, which may be important in the tunnel-building interaction analysis. For example, consider the case where the tunnel is located directly beneath the building centreline; vertical displacements drag the building downwards and, at the same time, horizontal displacements pull the portion of the building above the tunnel (at the ground or foundation level) horizontally towards its centre. The horizontal displacements act to compress the building horizontally and increase its resistance against bending deformations (because of the compression applied at the bottom fibre), thereby increasing its resistance to vertical displacements.

The interaction between vertical and horizontal displacements of both the soil and the structure is illustrated in Figures 7a and b for two buildings (Cases 3 and 5 from Table 1). These figures show building displacements from analyses where only vertical S_v, only horizontal S_h, or both S_v and S_h were applied to the models. Interestingly, the application of both vertical and horizontal soil movements results in a smaller building maximum vertical displacement compared to the analysis for only S_v; this is consistent with the upwards building deflections obtained when only S_h was applied (due to the compressive action of S_h). Also note that for the stiffer Case 5 building the interaction effects between vertical and horizontal input soil displacements is minimal.

Figures 7c and d show the horizontal strains, ϵ_h, induced in the building. There is a significant difference between the case where both displacement components are applied and when they are applied separately. When the

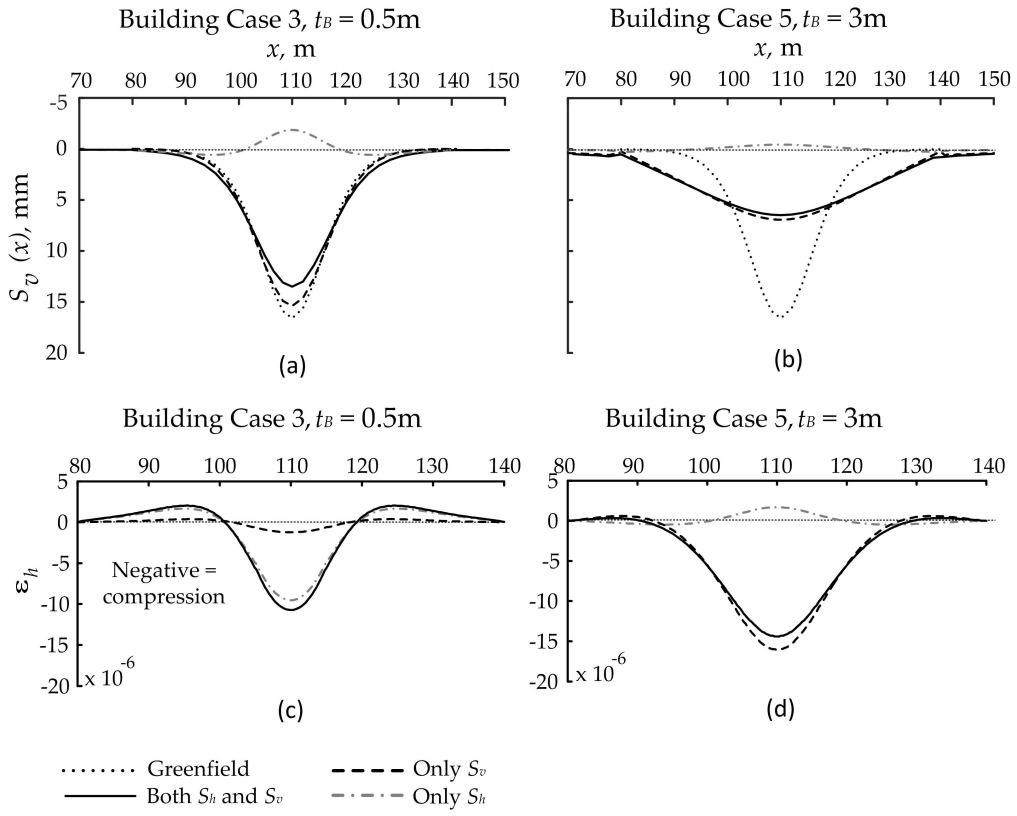

Figure 7: Effect of applying ground displacement components separately to a model: (a) and (b) ground displacements in the presence of a building; (c) and (d) horizontal strains created in the building. Tunnel volume loss = 1.76%

building is flexible (i.e. beam thickness is small; Figure 7c), most of the effect of S_h is transferred to the building and horizontal strains due to vertical displacements play a minor role, hence the 'Only S_h' line matches closely with the case where both displacements are applied. As bending stiffness of the building increases (i.e. larger beam thickness; Figure 7d), the resistance of the building against deformations (bending and axial) increases. Because axial stiffness is significant, only a minimal axial effect is transferred from the soil to the building. Tensile horizontal strains occur at the middle of the beam because of the coupling between beam bending and soil horizontal ground movements. On the other hand, when S_v and S_h are applied together, significant compressive horizontal strains are induced due to the action of S_v.

In scenarios where the tunnel is located below the edge or outside the building plan area (i.e. $e/L_{bldg} \geq 0.5$), analysis results indicated a negligible tendency of horizontal movements to reduce vertical displacements (i.e. no practical difference was found when both S_h and S_v were applied and when only S_v was applied to the model). This outcome relates to the end constraints of the building, which affects its ability to resist deformations. Further discussion on this aspect is given later in the paper.

It is worth noting that when equivalent beams are used instead of actual buildings, there will be a coupling effect between the cross sectional flexural (EI) and axial (EA) rigidity of the beam on the axial and bending behaviour. For a specific beam length, a change in the thickness leads to a change in the bending and axial behaviour of the beam. A larger axial effect is transferred to the beam when the axial rigidity decreases. Similarly, the beam experiences a larger bending effect when flexural rigidity reduces. This change may alter

the behaviour of the beam to some extent due to the occurrence of the coupling effect between EI and EA. For instance, a decrease in EA induces larger horizontal displacements in the beam which in turn results in larger compressive stresses that may reduce vertical displacements. To understand this effect clearly, beams should be analysed for both cases of having constant EA with variable EI, and constant EI with variable EA, as done by Potts and Addenbrooke (1997). However, this issue does not have an effect on the comparative results reported here since this feature is present in both the conventional numerical and mixed E–N analyses. Furthermore, investigating the impact of using equivalent beams rather than the actual building is not the focus of this paper.

In the following sections, unless otherwise stated, results are based on analyses where both S_h and S_v were applied together to investigate the effect of building stiffness on ground displacements caused by tunnelling.

7. Comparison of mixed E–N with numerical results

Results presented in this section are based on three cases of tunnel location: $e/L_{bldg} = 0$, 0.5 and 0.75. Results relate to cases with $C/D_t = 2.4$ with $V_{ls,surf}$ = 1.55% or $C/D_t = 4.4$ with $V_{ls,surf} = 2.77\%$.

7.1. Bending modification factors for $e/L_{bldg} = 0$

Figure 8 presents bending modification factors from conventional numerical and mixed E–N analyses for $e/L_{bldg} = 0$, 0.5 and 0.75 and for two tunnel depths of $C/D_t = 2.4$ and 4.4. For the case of $e/L_{bldg} = 0$ when C/D_t = 2.4, Figure 8a shows that the bending modification factors from the mixed E–N method are generally lower than those from the conventional numerical

analysis. The difference is small for low values of relative bending stiffness and increases as the relative bending stiffness increases.

The results in Figure 8a indicate that ground displacements due to tunnelling have less of an effect on buildings based on the mixed E–N method compared to the conventional numerical analyses; i.e. buildings in the mixed E–N method have a greater relative structure-soil stiffness and are less affected by ground displacements compared to the conventional numerical analyses. The reason for this relates to the relative position and extent of the building in relation to the extent of the greenfield settlement trough, which is depicted in Figure 9a. The building with $e/L_{bldg} = 0$ extends a considerable distance past the extent of the mixed E–N greenfield settlement trough, whereas it is inside the greenfield settlement trough for the conventional numerical model. The section of the building located outside the affected soil zone in the mixed E–N analysis provides support to the section of the building affected by soil displacements (like a fixed end support that prevents rotation at the location where the building first becomes affected by ground movements), thereby increasing the building's resistance to deformation. This feature is not explicitly captured by the relative stiffness equations proposed by Potts and Addenbrooke (1997) and Franzius et al. (2006).

Figure 9b illustrates that greenfield horizontal movements in the conventional numerical analyses are greater over a wider area compared to the mixed E–N analyses (for $e/L_{bldg} = 0$). The effect of the resulting compression applied to the building, which contributes to the resistance of the building against bending, is therefore more pronounced in the conventional numerical analyses compared to the mixed E–N analyses. The horizontal displacements

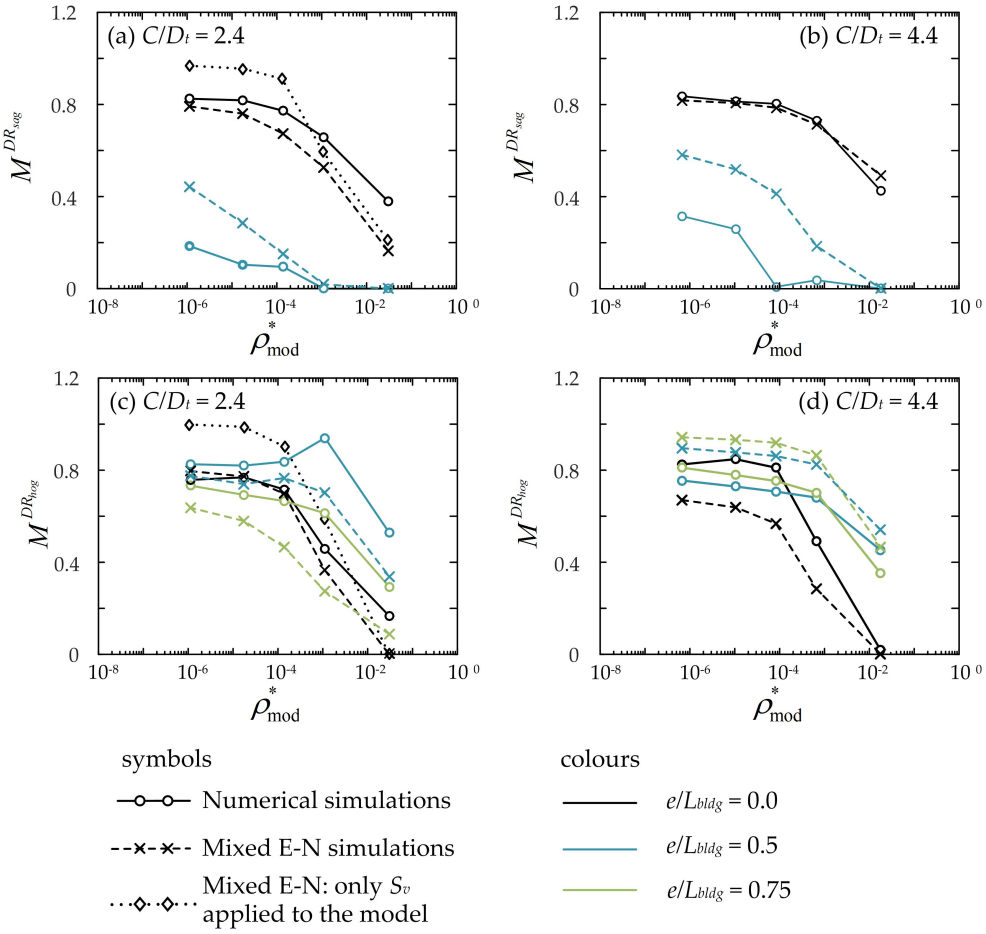

Figure 8: Comparison of bending modification factors between conventional numerical and mixed E–N methods for $V_{ls,surf} = 1.55\%$ and 2.77% for C/D_t =2.4 and 4.4, respectively

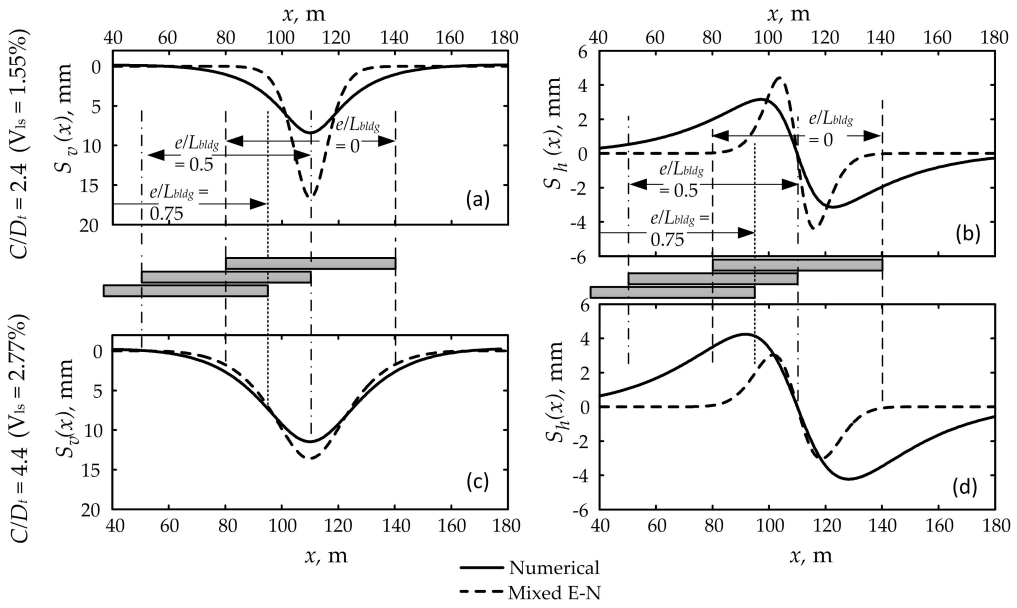

Figure 9: Tunnelling induced surface greenfield movements predicted by conventional numerical and mixed $E - N$ methods

outside the building area in the conventional numerical analyses (which do not exist in the mixed E–N analyses) also increase the building resistance against bending deformations.

To demonstrate how horizontal displacements influence the value of bending modification factors, mixed E–N simulations were performed where only vertical displacements were included for the case $C/D_t = 2.4$, as shown in Figures 8a and c. The data show that exclusion of horizontal displacements (only S_v) results in larger values of M^{DR} (greater deformation of the building) compared to the case where both S_h and S_v were applied. The additional deformation of the building was also demonstrated in Figures 7a and b where excluding S_h effectively removed a component of upwards beam deflection. Note that the effects of horizontal displacements on building deformations were also reported by Potts and Addenbrooke (1997) in their numerical analyses and Farrell et al. (2014) based on geotechnical centrifuge tests.

For the case of $C/D_t = 4.4$ and $e/L_{bldg} = 0$, the values of $M^{DR_{sag}}$ computed from both conventional numerical and mixed E–N analyses are very similar, as shown in Figure 8b. This indicates similar building effects on ground displacements despite the slightly narrower settlement trough in the mixed E–N analyses, as displayed in Figure 9c. This is mainly due to the existence of large horizontal displacements beneath and adjacent to the building in the conventional numerical analyses (Figure 9d), which counteract the reduction of relative bending stiffness caused by the wider settlement trough.

In terms of $M^{DR_{hog}}$ for $e/L_{bldg} = 0$, the mixed E–N analysis outcomes are generally lower than those from the numerical simulations. The difference is relatively small for the case of $C/D_t = 2.4$ (Figure 8c) but more pronounced

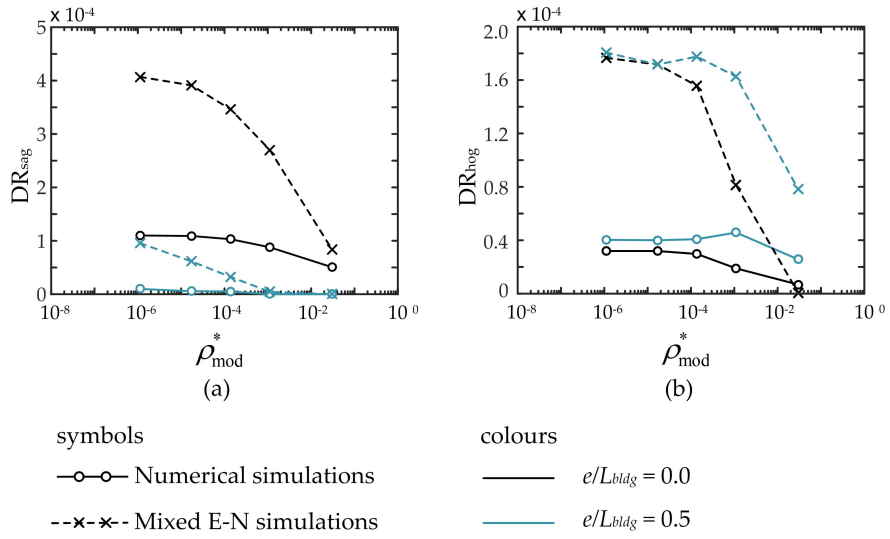

Figure 10: Comparison of (a) sagging and (b) hogging deflection ratios obtained from conventional numerical and mixed E–N analyses for $C/D_t = 2.4$ and $V_{ls,surf} = 1.55\%$

for $C/D_t = 4.4$ (Figure 8d). This again illustrates that buildings in the mixed E–N analyses showed greater relative structure-soil bending stiffness than in the conventional numerical analyses. This is because the narrower settlement trough in the mixed E–N analyses has a proportionally higher impact (increase) on the resulting relative stiffness than the effect of the difference in horizontal displacements between the two analyses for the case of $e/L_{bldg} = 0$.

The calculation of M^{DR} includes a normalisation against the greenfield displacements, hence it does not fully demonstrate the effect of the different greenfield settlement trough inputs within the conventional numerical and mixed E–N analyses. The level of flexural distortion of the structure estimated by the two methods varies considerably more than indicated in the M^{DR} data. For instance, Figure 10 shows that the deflection ratios, DR, in the

sagging and hogging zones calculated with the mixed E–N analyses are notably higher than those from the conventional numerical analyses for $C/D_t = 2.4$, especially at low values of relative bending stiffness. The same observation applies for the case of $e/L_{bldg} = 0.5$. The potential for building damage is proportional to deflection ratio (Mair et al., 1996) rather than modification factor, hence these results illustrate the importance of correctly estimating and incorporating greenfield ground displacements within preliminary risk assessments and numerical analyses.

7.2. Bending modification factors for $e/L_{bldg} > 0$

For the cases where the tunnel was not located under the building centreline ($e/L_{bldg} = 0.5$ and 0.75), it is important to describe the effects of the rotational constraint provided by the soil outside the tunnel influence area, where settlements are low. Figure 11 illustrates how building length affects results for $e/L_{bldg} = 0.5$ and $C/D_t = 2.4$. Two building lengths are considered: 60 m (where the building extends far outside the greenfield displacement profile), and 30 m (where most of the building is affected by greenfield displacements).

The portion of the 60 m building outside the displacement zone provides a degree of constraint to the deformed part of the building, which reduces rotation (i.e. tilting of entire building) but results in greater distortion (i.e. bending strains) compared to the 30 m building, which undergoes significant rotation but little distortion. The resistance of a building to rotation is important when considering its response to ground displacements; as building length increases outside the displaced soil zone, so does its ability to resist rotation. Note that for the symmetric case where $e/L_{bldg} = 0$, rotation is not permitted and therefore the building bending stiffness is relatively high.

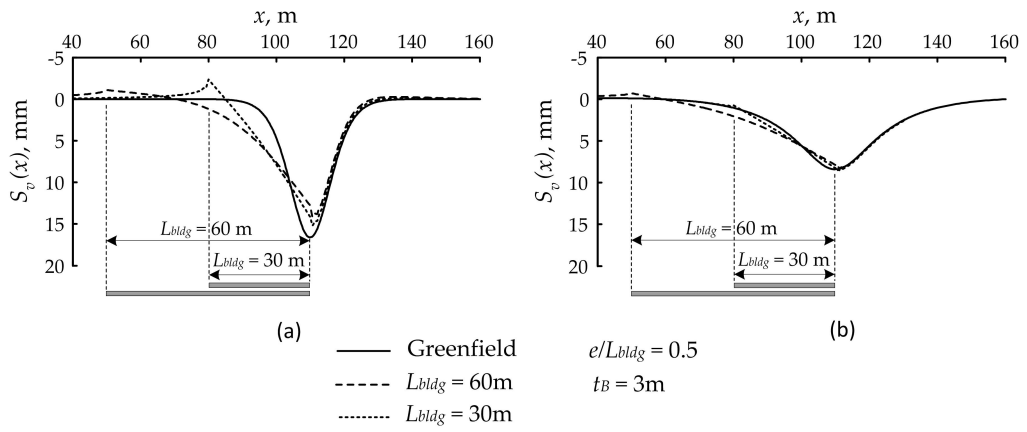

Figure 11: Effect of building length on ground displacements due to tunnelling for $C/D_t = 2.40$: (a) mixed $E-N$ and (b) conventional numerical analyses

Haji et al. (2018) explained the parameters that affect the bending stiffness of a member and illustrated the importance of considering the effect of the building lengths both within and outside the displaced soil zones. Currently available methods for evaluating relative stiffness do not account for the effect of building length in relation to the displaced soil zone; this is an area of research that would benefit from additional attention.

For $e/L_{bldg} = 0.5$ and 0.75, Figure 8a and b show that values of $M^{DR_{sag}}$ from the mixed E–N method for $C/D_t = 2.4$ and 4.4 are higher than those from the conventional numerical analyses. Values of $M^{DR_{sag}}$ indicate stiffer buildings (relative to the soil) in the conventional numerical analyses because of the action of the large horizontal displacements in the conventional numerical analyses, which causes a significant increase to the building's resistance to bending deformations.

The values of $M^{DR_{hog}}$ from the mixed E–N analyses are generally lower than those from the conventional numerical analyses for $e/L_{bldg} = 0.5$, 0.75 and

$C/D_t = 2.4$, especially for higher values of relative bending stiffness, as shown in Figure 8c. There is an interesting transition point observable in Figure 8c for the conventional numerical analysis results at about $\rho^*_{mod} \geq 1.1 \times 10^{-3}$, where hogging occurs in the entire building length (corresponding to the point where $M^{DR_{sag}} = 0$ in Figure 8a), resulting in a marked increase of $M^{DR_{hog}}$.

A different trend of $M^{DR_{hog}}$ is obtained for $C/D_t = 4.4$ (Figure 8d), where values from the mixed E–N analyses are higher than the conventional numerical analyses. Since vertical greenfield displacements from both methods are similar (see Figure 9c), the greater ability of the conventional numerical analysis buildings to resist hogging zone distortions (i.e. lower values of $M^{DR_{hog}}$) must be due to the effect of the larger magnitude and wider profile of the greenfield horizontal displacements in the conventional numerical analyses.

7.3. Axial modification factors

Figure 12 presents the axial modification factors from the conventional numerical and mixed E–N analyses for $e/L_{bldg} = 0$, 0.5 and 0.75, and $C/D_t = 2.4$, 4.4. Figure 12a and b present the compressive strain modification factors $M^{\epsilon_{hc}}$; Figure 12c and d give the tensile modification factors, $M^{\epsilon_{ht}}$. For $e/L_{bldg} = 0$, the data show that the conventional numerical analysis results for $M^{\epsilon_{hc}}$ are larger than those of the mixed E–N analyses, whereas $M^{\epsilon_{ht}}$ values are smaller (for both $C/D_t = 2.4$ and 4.4). The difference in modification factors between the conventional numerical and mixed E–N analyses decreases with the increase in relative axial stiffness factor.

To help understand the different axial responses from the two methods, it is important to note that the greenfield soil is in compression horizontally

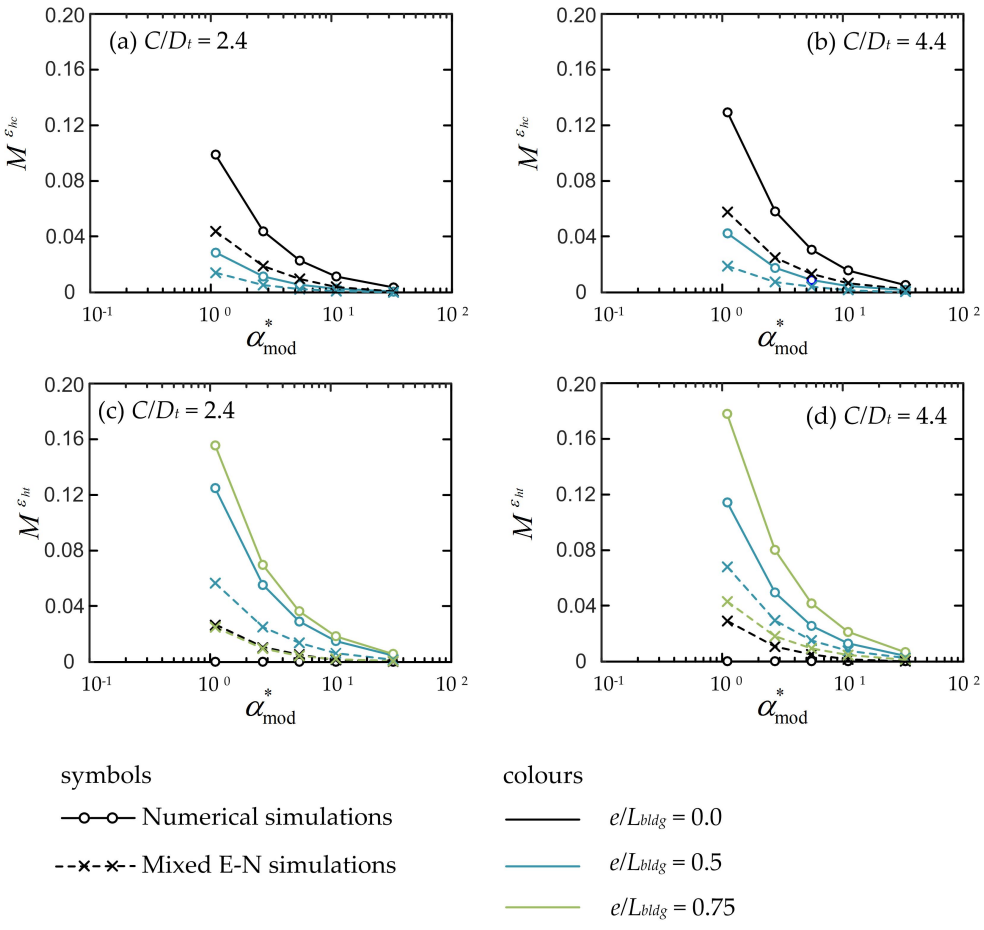

Figure 12: Comparison of axial modification factors between conventional numerical and mixed E–N methods for $C/D_t = 2.4$ ($V_{ls,surf} = 1.55\%$) and $C/D_t = 4.4$ ($V_{ls,surf} = 2.77\%$)

within the zone bounded by the peak values of S_h, and in tension outside this region. As shown in Figure 9b and d, for structures with $e/L_{bldg} = 0$, the greenfield displacement profile from the conventional numerical analysis encompasses the entire building. The effect is that the building is completely in compression and values of $M^{\epsilon_{hc}}$ are greater for the conventional numerical analysis than the mixed E–N method (Figure 12a, b). In the mixed E–N method, peak horizontal displacements are closer to the tunnel centreline and the structure is subjected to both tensile and compressive forces from the soil. This produces values of $M^{\epsilon_{ht}}$ (tension) from the mixed E–N method that are greater than zero for the considered configurations (Figure 12c, d).

For the case of $e/L_{bldg} > 0$, Figure 12 shows that both $M^{\epsilon_{hc}}$ and $M^{\epsilon_{ht}}$ from the conventional numerical analyses are larger than those from the mixed E–N analyses for both $C/D_t = 2.4$ and 4.4. The high values of axial modification factors from the conventional numerical analyses is mainly related to the effect of the proportion of the building located inside the displaced soil zone, which as a result experiences more axial distortion from horizontal ground displacements than buildings in the mixed E–N analyses where the horizontal displacement profile is narrower (see Figure 9).

8. Conclusions

A mixed empirical-numerical (mixed E–N) method to predict the response of buildings to realistic inputs of tunnelling induced ground movements was presented in the paper. A modified semi-analytical method was used to obtain the greenfield displacements in the paper, however any input could be incorporated into the methodology. The input greenfield displacements

were based on centrifuge test data and included both horizontal and vertical displacements. The mixed E–N method allows the application of horizontal and vertical displacements to the model either together or separately, thereby allowing a detailed evaluation of the coupling effect of the two displacements. Results obtained from the proposed mixed E–N method were compared against conventional numerical analyses in which the tunnel was simulated, resulting in wider settlement troughs and greater horizontal displacements than expected in reality. It was shown that the action of the unrealistic horizontal displacements in the conventional numerical analyses increased the resistance of the building against bending deformations quite considerably in some scenarios.

With regard to bending modification factors when $e/L_{bldg} = 0$, it was shown that buildings in the mixed E–N analyses were distorted slightly less by ground displacements compared to buildings in the conventional numerical analyses for the sagging and hogging zones. Moreover, higher tensile and lower compressive strains were induced in buildings in the mixed E–N analyses compared to the conventional numerical simulations (no tensile strains were produced in the conventional numerical analyses due to the very wide horizontal displacement profile).

For eccentric buildings, there was no practical difference between the bending modification factors of the mixed E–N and conventional numerical analyses in the hogging zone while modification factors of the sagging zone in the mixed E–N analyses were significantly higher than those from the conventional numerical analyses. Furthermore, both axial modification factors (compressive and tensile) computed from the mixed E–N method were lower

than those estimated from the conventional numerical analyses.

Comparison of deflection ratios between the conventional numerical and mixed E–N methods showed that buildings in the mixed E–N method were distorted by tunnelling induced ground displacements to a greater extent than buildings in the conventional numerical analyses. This demonstrated the importance of incorporating accurate inputs of greenfield ground movements within numerical analyses of tunnel-building interaction.

A. Semi–analytical method for estimating greenfield displacements in sand

The semi-analytical solution for horizontal (S_h) and vertical (S_v) displacements proposed by Franza and Marshall (2015) is given by:

$$S_v = -2\varepsilon R_t^2 \zeta \left[\frac{z_1}{2r_1^2}\left(1 - \frac{x^2 - z_1^2}{r_1^2}\right) - \frac{z_2}{2r_2^2}\left(1 + \frac{x^2 - z_2^2}{r_2^2}\right) + \frac{1}{2r_2^4}\left(2(z + z_t)(x^2 - z_2^2) + 4z_t z z_2 \frac{3x^2 - z_2^2}{r_2^2}\right)\right] \tag{5}$$

$$S_h = -2\varepsilon R_t^2 \zeta \left[\frac{x}{2r_1^2}\left(1 - \frac{x^2 - z_1^2}{r_1^2}\right) + \frac{x}{2r_2^2}\left(1 - \frac{x^2 - z_2^2}{r_2^2}\right) - \frac{4xz}{2r_2^4}\left(z_2 - \frac{z_t\left(x^2 - 3z_2^2\right)}{r_2^2}\right)\right] \tag{6}$$

$$\zeta = c_A \exp\left\{ -\left[c_1 \left(\frac{z}{z_t}\right)^2 + c_2 \left(\frac{x}{z_t}\right)^2 \right] \right\} + \quad c_B \exp\left\{ -\left[c_3 \left(\frac{z}{z_t} - c_4\right)^2 + c_3 \left(\frac{x}{z_t}\right)^2 \right] \right\} \tag{7}$$

where $z_1 = z - z_t$, $z_2 = z + z_t$, $r_1 = \sqrt{x^2 + z_1^2}$, $r_2 = \sqrt{x^2 + z_2^2}$, $\varepsilon = V_{lt}/(2 \times 100)$ is the tunnel convergence parameter, V_{lt} is the tunnel volume loss expressed in percentage, R_t is the tunnel radius, and ζ is the corrective term whose coefficients, c_i, depend linearly on V_{lt} (i.e. $c_i = m_i V_{lt} + q_i$).

These equations illustrate the effects of tunnel volume loss on soil deformation patterns. However, the coefficients of ζ in Franza and Marshall (2015) were calibrated on the outcomes of a single centrifuge test with $C/D_t = 2.4$ and a soil relative density of 90% (obtained from Marshall et al. 2012). Therefore, the solution has limited applicability.

The semi-analytical approach presented in Franza and Marshall (2015)

was extended based on a wider set of centrifuge data, including the effects of cover to diameter ratio, C/D_t, and soil relative density, I_d. Because the ground movement distribution may be narrower or wider than the elastic deformation pattern, depending on C/D_t and I_d, the expression for the corrective term ζ was modified with two additional coefficients (c_5 and c_6) to allow for more adaptable curve-fitting. Furthermore, to improve the curve-fitting of horizontal movements, two different corrective terms, ζ_v and ζ_h, displayed in Equation 8, were implemented in the vertical and horizontal direction, respectively. The adopted coefficients are listed in Table 3.

$$\begin{aligned}
\zeta_v =& c_{A,v} \exp\left\{-\left[c_{1,v}\left(\frac{z}{z_t}\right)^2 + c_{2,v}\left(\frac{x}{z_t}\right)^2 + c_{6,v}\left(\frac{x}{z_t}\right)^4\right]\right\} \\
&+ c_{B,v} \exp\left\{-\left[c_{3,v}\left(\frac{z}{z_t} - c_{4,v}\right)^2 + c_{5,v}\left(\frac{x}{z_t}\right)^2\right]\right\} \\
\zeta_h =& c_{A,h} \exp\left\{-\left[c_{1,h}\left(\frac{z}{z_t}\right)^2 + c_{2,h}\left(\frac{x}{z_t}\right)^2 + c_{6,h}\left(\frac{x}{z_t}\right)^4\right]\right\} \\
&+ c_{B,h} \exp\left\{-\left[c_{3,h}\left(\frac{z}{z_t} - c_{4,h}\right)^2 + c_{5,h}\left(\frac{x}{z_t}\right)^2\right]\right\}
\end{aligned} \tag{8}$$

$$\begin{aligned}
C_A &= m_{a,i} \times V_{lt} + q_{a,i} \\
C_B &= m_{b,i} \times V_{lt} + q_{b,i} \\
c_i &= m_i \times V_{lt} + q_i
\end{aligned} \tag{9}$$

$$\begin{aligned}
C_{Ax} &= m_{ax,i} \times V_{lt} + q_{ax,i} \\
C_{Bx} &= m_{bx,i} \times V_{lt} + q_{bx,i} \\
c_{ix} &= m_{ix} \times V_{lt} + q_{ix}
\end{aligned} \tag{10}$$

Table 3: The adopted coefficients for semi–analytical approach

I_d	0.9	0.9
C/D_t	2.4	4.4
m_a	-0.16	-0.15
q_a	1.46	1.89
m_b	0.20	0.03
q_b	0	0
m_1	0.11	0
q_1	1.38	1.11
m_2	0.14	0.14
q_2	0.05	-0.40
m_3	1.18	16.75
q_3	0	0
m_4	0	0
q_4	0.83	0.90
m_5	11.53	1.00
q_5	0	0
m_6	0	0
q_6	0.10	0.10
m_{ax}	-0.16	-0.15
q_{ax}	1.46	1.89
m_{bx}	0.20	0.03
q_{bx}	0	0
m_{1x}	0	0.48
q_{1x}	7.06	5.01
m_{2x}	-0.03	-0.36
q_{2x}	1.40	2.43
m_{3x}	1.18	16.75
q_{3x}	0	0
m_{4x}	0	0
q_{4x}	0.83	0.90
m_{5x}	11.53	1.00
q_{5x}	0	0
m_{6x}	0	0
q_{6x}	0.10	0.10

636 Addenbrooke, T. I., Potts, D. M., Puzrin, A. M., 1997. The influence of
637 pre-failure soil stiffness on the numerical analysis of tunnel construction.
638 Geotechnique 47 (3), 693–712.

639 Augarde, C. E., 1997. Numerical modelling of tunnelling processes for asses-
640 sment of damage to buildings. Ph.D. thesis, University of Oxford.

641 Bilotta, E., Paolillo, A., Russo, G., Aversa, S., 2017. Displacements induced
642 by tunnelling under a historical building. Tunnelling and Underground
643 Space Technology 61, 221–232.

644 Bowles, J. E., 1997. Foundation analysis and design, 5th Edition. McGraw-
645 Hill.

646 Cheng, C., Dasari, G., Chow, Y., Leung, C., 2007. Finite element analysis of
647 tunnel–soil–pile interaction using displacement controlled model. Tunnelling
648 and Underground Space Technology 22 (4), 450–466.

649 Dimmock, P. S., Mair, R. J., 2008. Effect of building stiffness on tunnelling-
650 induced ground movement. Tunnelling and Underground Space Technology
651 23 (4), 438–450.

652 Farrell, R., 2011. Tunnelling in sands and the response of buildings. Ph.D.
653 thesis, University of Cambridge.

654 Farrell, R., Mair, R., Sciotti, A., Pigorini, A., 2014. Building response to
655 tunnelling. Soils and Foundations 54 (3), 269–279.

656 Franza, A., 2016. Tunnelling and its effects on piles and piled structures.
657 Ph.D. thesis, University of Nottingham.

Franza, A., DeJong, M. J., 2017. A simple method to evaluate the response of structures with continuous or separated footings to tunnelling-induced movements. In: Proceeding of the Congress on Numerical Methods in Engineering 2017.

Franza, A., Marshall, A., 2015. Semi-analytical prediction of ground movements due to shallow tunnels in sand. Proceedings of the XVI ECSMGE - Geotechnical Engineering for Infrastructure and Development, 461–466.

Franzius, J., Potts, D., Burland, J., 2005. The influence of soil anisotropy and k0 on ground surface movements resulting from tunnel excavation. Géotechnique 55 (3), 189–199.

Franzius, J. N., Potts, D. M., Addenbrooke, T. I., Burland, J. B., 2004. The influence of building weight on tunnelling-induced ground and building deformation. Soils and Foundations 44 (1), 25–38.

Franzius, J. N., Potts, D. M., Burland, J. B., 2006. The response of surface structures to tunnel construction. Proceedings of the ICE-Geotechnical Engineering 159 (1), 3–17.

Giardina, G., DeJong, M. J., Mair, R. J., 2015. Interaction between surface structures and tunnelling in sand: Centrifuge and computational modelling. Tunnelling and Underground Space Technology 50, 465–478.

Goh, K., Mair, R., 2011. The horizontal response of framed buildings on individual footings to excavation-induced movements. In: Proceedings of 7th International Symposium on Geotechnical Aspects of Underground Construction in Soft Ground, May, Rome.

681 Goh, K. H., Mair, R. J., 2014. Response of framed buildings to excavation-
682 induced movements. Soils and Foundations 54 (3), 250–268.

683 Haji, T. K., Marshall, A. M., Tizani, W., 2018. A cantilever approach to
684 estimate bending stiffness of buildings affected by tunnelling. Tunnelling
685 and Underground Space Technology 71, 47–61.

686 Jurecic, N., Zdravkovic, L., Jovicic, V., 2013. Predicting ground movements in
687 london clay. Proceedings of the Institution of Civil Engineers-Geotechnical
688 engineering 166 (5), 466–482.

689 Klar, A., Marshall, A. M., 2008. Shell versus beam representation of pipes in
690 the evaluation of tunneling effects on pipelines. Tunnelling and Underground
691 Space Technology 23 (4), 431–437.

692 Mair, R., 2013. Tunnelling and deep excavations: Ground movements and their
693 effects. In: Proc., 15th European Conf. on Soil Mechanics and Geotechnical
694 Engineering–Geotechnics of Hard Soils–Weak Rocks (Part 4). IOS Press,
695 Amsterdam, pp. 39–70.

696 Mair, R., Gunn, M., O'REILLY, M., 1982. Ground movement around shallow
697 tunnels in soft clay. Tunnels & Tunnelling International 14 (5).

698 Mair, R., Taylor, R., 1997. Theme lecture: Bored tunnelling in the urban
699 environment. 14th international conference on soil mechanics and foundation
700 engineering 4, 2353–2385.

701 Mair, R., Taylor, R., Burland, J., 1996. Prediction of ground movements and
702 assessment of risk of building damage due to bored tunnelling. In: Fourth

International Symposium of International Conference of Geotechnical Aspects of on Underground Construction in Soft Ground. AA Balkema, pp. 713–718.

Maleki, M., Sereshteh, H., Mousivand, M., Bayat, M., 2011. An equivalent beam model for the analysis of tunnel-building interaction. Tunnelling and Underground Space Technology 26 (4), 524–533.

Marshall, A., Elkayam, I., Klar, A., Mair, R., 2010. Centrifuge and discrete element modelling of tunnelling effects on pipelines. In: Proceedings of the 7th International Conference on Physical Modelling in Geotechnics. pp. 633–637.

Marshall, A., Farrell, R., Klar, A., Mair, R., 2012. Tunnels in sands: the effect of size, depth and volume loss on greenfield displacements. Geotechnique 62 (5), 385–399.

Marshall, A. M., Franza, A., 2017. Discussion of 'observation of ground movement with existing pile groups due to tunneling in sand using centrifuge modelling' by ittichai boonsiri and jiro takemura. Geotechnical and Geological Engineering 35 (1), 535–539.

Potts, D., Addenbrooke, T., 1997. A structure's influence on tunnelling-induced ground movements. Proceedings of the ICE-Geotechnical Engineering 125 (2), 109–125.

Selby, A., 1999. Tunnelling in soils–ground movements, and damage to buildings in workington, uk. Geotechnical & Geological Engineering 17 (3-4), 351–371.

726 SIMULIA, A., 2012. 6.12. ABAQUS Analysis User's Manual.

727 Tan, F. S. C., 1990. Centrifuge and theoretical modelling of conical footings
728 on sand. Ph.D thesis, Cambridge Univ.

729 Vermeer, P. A., Borst, D. R., 1984. Non-associated plasticity for soils, concrete
730 and rock. HERON, 29 (3), 1984.

731 Verruijt, A., Booker, J., 1996. Surface settlements due to deformation of a
732 tunnel in an elastic half plane. Geotechnique 46 (4), 753–756.

733 Wang, Y., Shi, J., Ng, C. W., 2011. Numerical modeling of tunneling effect
734 on buried pipelines. Canadian Geotechnical Journal 48 (7), 1125–1137.

735 Zhao, Y., 2008. In situ soil testing for foundation performance prediction.
736 Ph.D. thesis, University of Cambridge.

737 Zhou, B., 2014. Tunnelling-induced ground displacements in sand. Ph.D.
738 thesis, University of Nottingham.

739 Zhou, B., Marshall, A. M., Yu, H.-S., 2014. Effect of relative density on
740 settlements above tunnels in sands. In: Geo-Shanghai 2014.